Confinement-Induced Self-Pumping in 3D Active Fluids

Minu Varghese, Arvind Baskaran, Michael F. Hagan, and Aparna Baskaran
Martin Fisher School of Physics, Brandeis University, Waltham, Massachusetts 02453, USA

(Received 17 July 2020; revised 25 September 2020; accepted 24 November 2020; published 29 December 2020)

Two dimensional active fluids display a transition from turbulent to coherent flow upon decreasing the size of the confining geometry. A recent experiment suggests that the behavior in three dimensions is remarkably different; emergent flows transition from turbulence to coherence upon *increasing* the confinement height to match the width. Using a simple hydrodynamic model of a suspension of extensile rodlike units, we provide the theoretical explanation for this puzzling behavior. Furthermore, using extensive numerical simulations supported by theoretical arguments, we map out the conditions that lead to coherent flows and elucidate the critical role played by the aspect ratio of the confining channel. The mechanism that we identify applies to a large class of symmetries and propulsion mechanisms, leading to a unified set of design principles for self-pumping 3D active fluids.

DOI: 10.1103/PhysRevLett.125.268003

Active matter describes systems whose constituent particles consume energy to drive motion or generate forces [1–14]. Being continuously driven far from equilibrium, active materials can exhibit spectacular spatiotemporal behaviors not possible in equilibrium systems. One such example is "self-pumping" flow, in which confining an active fluid leads to a spontaneous coherent flow, enabling advected material transport in the absence of any external driving such as a pressure gradient [15]. Harnessing coherent spontaneous flow at scales relevant to practical devices would enable converting particle-scale chemical energy into macroscopic productive work, and thus has tremendous potential for practical applications. However, the mechanisms that drive and control self-pumping of confined active fluids are insufficiently understood to design such devices.

Spontaneous flow has been reported in diverse active fluids, including suspensions of microswimmers [16–23], cell monolayers [24,25], and active gels built from subcellular components [26–29]. At the microscopic level, some of these systems have polar symmetry [16,18–23], and others have nematic symmetry [24–29]. Nevertheless, a unifying feature of all these systems is that they are composed of force dipoles in a fluid. In this work, we show that flow generated by force dipoles together with flow alignment and confinement give rise to system-size dependent length scales in the structure of the flow, which can be harnessed to induce coherent flows in diverse systems. In particular, we uncover the underlying physics of aspect-ratio-dependent coherent flows observed in dilute isotropic suspensions of extensile microtubule bundles powered by ATP-driven molecular motors [29].

Most previous theoretical studies of active matter, with a few notable exceptions[16,30], have considered models with polar self-propelled constituents [8,19,21,31–39], or mutually aligning nematic constituents [1–14,26]. Therefore, at least one of these ingredients—self-propulsion or aligning interactions—is often thought to be required for spontaneous flows. However, experiments by Wu *et al.* [29] demonstrated emergent flows in meter long channels with no orientational order, i.e., well below the isotropic-nematic (IN) transition density of the microtubule bundles. Moreover, the coherence of the flow was nonmonotonic as the size of the channel was varied, occurring only in channels with low aspect ratio cross sections: $1/2 \leq H/W \leq 2$, with H and W the height and width of the channel. This transition to spontaneous flow is thus an intrinsically 3D behavior, which cannot be explained by 2D models of active nematics [40–43].

Here, we show that a minimal theoretical description of extensile microtubules below their IN transition, which includes only the force-dipole and flow-aligning character of the bundles, exhibits a transition to self-pumping flow that depends critically on dimensionality. We then reveal the physical origins of this behavior by formulating the aspect ratio dependence in terms of a confinement-induced length scale in the structure of the flow. Finally, we propose design principles for generating self-pumping flows in active fluids. The simplicity of our model implies that these design principles apply to a wide variety of seemingly disparate active matter systems.

Model.—Consider N noninteracting ellipsoids, each of length l and diameter b suspended in a fluid in d dimensions. The center of mass of ellipsoid i, $\vec{r}_i$, evolves as $\partial_t \vec{r}_i = \vec{u}(\vec{r}_i) + \sqrt{2\kappa}\vec{\eta}^T(\vec{r}_i)$, where $\vec{u}(\vec{r})$ is the fluid velocity at position $\vec{r}$, η_α^T is a stochastic Gaussian white noise, and κ is the translational diffusion constant. Let the axis of orientation of this ellipsoid, $\pm\hat{\nu}_i$ be defined along its axis of symmetry (length). In low Reynolds number flows, the time evolution of $\hat{\nu}_i$ is given by [44,45]

 © 2020 American Physical Society

$$\partial_t \hat{\nu}_i = \boldsymbol{\Omega}(\vec{r}_i)\cdot\hat{\nu}_i + \lambda(\boldsymbol{I}-\hat{\nu}_i\hat{\nu}_i)\cdot\mathbf{E}(\vec{r}_i)\cdot\hat{\nu}_i + \sqrt{\gamma/2}(\boldsymbol{I}-\hat{\nu}_i\hat{\nu}_i)\cdot\vec{\eta}^R(\vec{r}_i), \quad (1)$$

where $\Omega_{\alpha\beta}=\frac{1}{2}(\partial_\beta u_\alpha-\partial_\alpha u_\beta)$ and $E_{\alpha\beta}=\frac{1}{2}(\partial_\beta u_\alpha+\partial_\alpha u_\beta)$ represent spatial variations in the flow, $\lambda=[(l^2-b^2)/(l^2+b^2)]$, $\vec{\eta}^R$ is a Gaussian white noise, and γ is the rotational diffusion constant.

Suppose the ellipsoids are *active*, pushing outward along their axes with a force f and generating low Reynolds number flows around them. The emergent flow $\vec{u}$ is then a solution of the driven Stokes equation, $\eta\nabla^2\vec{u}(\vec{r})-\vec{\nabla}p=f\sum_i\hat{\nu}_i[\delta(\vec{r}-\vec{r}_i-l/2\hat{\nu}_i)-\delta(\vec{r}-\vec{r}_i+l/2\hat{\nu}_i)]$, [46] where η is the coefficient of viscosity and the mechanical pressure p is such that flows are incompressible: $\vec{\nabla}\cdot\vec{u}=0$.

We can coarse grain this microscopic model to derive the dynamical description of this fluid on long length scales. This gives the dynamics of the coarse-grained nematic order, $\boldsymbol{Q}=\langle\hat{\nu}\hat{\nu}-(\boldsymbol{I}/d)\rangle$, to be of the form (see Supplemental Material for derivation [47–50])

$$\partial_t\boldsymbol{Q}+\vec{u}\cdot\vec{\nabla}\boldsymbol{Q}+\boldsymbol{Q}\cdot\boldsymbol{\Omega}-\boldsymbol{\Omega}\cdot\boldsymbol{Q}=-\gamma\boldsymbol{Q}+\kappa\nabla^2\boldsymbol{Q}+\lambda\left[\frac{2}{d}\boldsymbol{E}+\boldsymbol{Q}\cdot\boldsymbol{E}+\boldsymbol{E}\cdot\boldsymbol{Q}-\frac{2}{d}\mathrm{tr}(\boldsymbol{Q}\cdot\boldsymbol{E})\boldsymbol{I}\right], \quad (2)$$

with $\eta\nabla^2\vec{u}-\vec{\nabla}p=\alpha\vec{\nabla}\cdot\boldsymbol{Q}$ and $\alpha=fl/2$. Note that our model is purely kinematic. Including passive nematic stresses in the Stokes equation would yield the Leslie-Erickson model for liquid crystals below the IN transition to linear order in $\boldsymbol{Q}$. This would decrease the effective activity [51], but not qualitatively change the phenomenology discussed here.

Mechanism for spontaneous flow.—Since $\gamma>0$, the only homogeneous state admitted by the model is $\boldsymbol{Q}=0$, $\vec{u}=0$. Consider fluctuations about this stationary isotropic state, $Q_{\alpha\beta}(\vec{r})=\int d\vec{k}\tilde{Q}_{\alpha\beta}(\vec{k})e^{-i\vec{k}.\vec{r}}$, and $u_\alpha(\vec{r})=\int d\vec{k}\tilde{u}_\alpha(\vec{k})e^{-i\vec{k}.\vec{r}}$. The effective dynamics of the flow is given by $\partial_t\tilde{u}_\beta=(i\alpha\hat{k}_\nu/\eta k)(\delta_{\beta\mu}-\hat{k}_\beta\hat{k}_\mu)\partial_t\tilde{Q}_{\mu\nu}$. Up to linear order in perturbations, $\partial_t\tilde{Q}_{\alpha\beta}=-(\gamma+\kappa k^2)\tilde{Q}_{\alpha\beta}-(i\lambda/d)(k_\alpha\tilde{u}_\beta+k_\beta\tilde{u}_\alpha)$. Eliminating $\tilde{Q}_{\alpha\beta}$, the effective linear dynamics of the flow is given by $\partial_t\tilde{u}_\beta=(-\gamma-\kappa k^2+\lambda\alpha/d\eta)\tilde{u}_\beta$. Thus, the stationary isotropic state is destabilized by long wavelength perturbations if $\alpha\lambda>d\eta\gamma$, i.e., if the ellipsoids are rodlike ($\lambda>0$) and the forces exerted by them are sufficiently extensile ($\alpha>0$), or if the ellipsoids are discoidal ($\lambda<0$) and the forces exerted by them are sufficiently contractile ($\alpha<0$) [8,19–22,30,52,53].

In this Letter, we will focus on extensile rodlike ellipsoids, to be consistent with experiments [29]. The phenomenology of contractile discoidal objects is identical, so we will not consider them separately. The emergence of spontaneous flows in a suspension of extensile rodlike objects can be ascribed to the following microscopic mechanism: (1) rodlike objects orient along the extensional axis of shear flows [Fig. 1(a)], while (2) shear flows generated by extensile rods have an extensional axis that coincides with the rod orientation [Fig. 1(b)]. If the relevant active timescale, $\tau_a=3\eta/\lambda\alpha$, is shorter than the timescale for loss of order due to rotational diffusion, $\tau_r=1/\gamma$, flows and nematic order at hydrodynamic scales arise spontaneously [21,30]. Thus, a positive reinforcement between shear alignment and extensile active flows destroys the isotropic state and generates the spontaneous flows discussed hereafter.

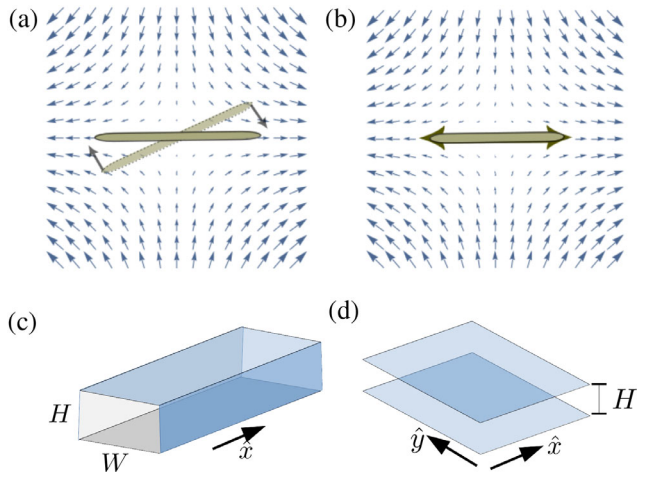

FIG. 1. (a) A slender rod aligns with the extensional axis of a shear flow; (b) flow field produced by an extensile rod; (c) confinement geometry for coherent flows; (d) confinement geometry for vortex size measurement.

In the rest of this Letter, we explore how confining walls can structure the spontaneous flows that are generated by the active shear alignment instability described above (see Supplemental Material [47] for full equations and numerical method [54–56]). The simplest theoretical setup that can sustain coherent flows is a 2D active fluid confined in a channel of width W. Above the flow alignment instability, strong confinements give rise to unidirectional coherent flows. As the width of the channel is increased, the flow becomes undulatory and finally turbulent. This is true regardless of anchoring at the walls (Supplemental Material [47]), and the steady states observed are similar to those discussed in the literature [15,42,57] for flows arising from the instability of orientationally ordered systems [15,46]. However, this phenomenology does not trivially extend to 3D.

Self-pumping in 3D.—To study the emergence of self-pumping flows in 3D, we assume a simple channel geometry with no slip walls at $y=0$, W and $z=0$, H [Fig. 1(c)], and no preferential anchoring (Neumann boundary conditions on $\boldsymbol{Q}$). The minimum channel dimensions that give rise to spontaneous flows are predicted by the stability analysis [solid white lines in Figs. 2(d) and 2(e)]. In channels with square cross sections, strong confinements above the instability yield self-pumping flows that are uniform along the length of the channel

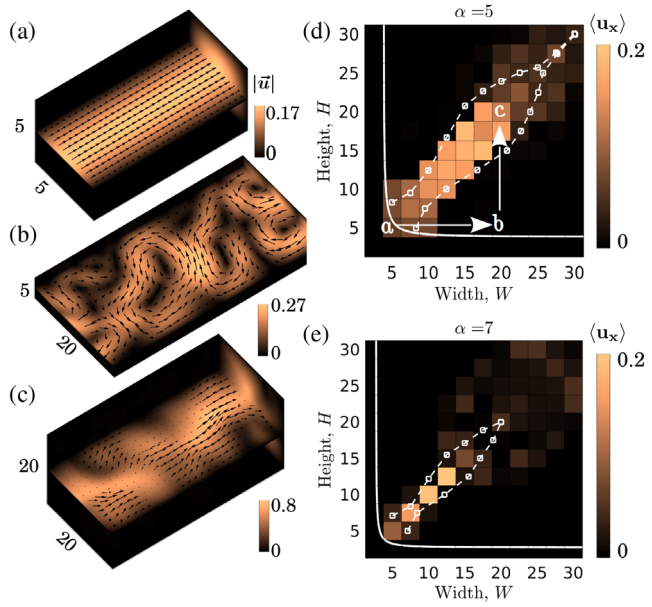

FIG. 2. Net flow along the channel varies nonmonotonically on monotonically increasing the cross-sectional area of the channel along the representative path (shown by arrows) in (d). (a)–(c) Instantaneous flow profiles to demonstrate the behavior shown by arrows in (d); when both the width and height of the channel are equal to 5 (a), the emergent flow is coherent and pumps fluid across the channel. When the width is increased to 20 (b), the flow loses coherence, and the average flow across the channel, $\langle u_x \rangle$ drops to zero. When the height is also increased to 20 (c), coherence is restored. (d),(e) Heat maps of average flow across the channel as a function of its dimensions for activity magnitude $\alpha = 5$ (d) and $\alpha = 7$ (e). The solid white line corresponds to the transition from stationary to flowing states predicted by the linear stability analysis. The dashed white lines encompass the region of coherent flows predicted by vortex sizes computed in [Fig. 3(d)].

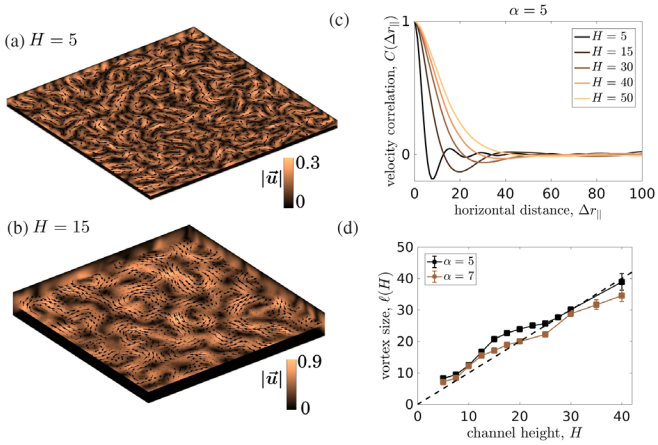

FIG. 3. (a),(b) Flow profile of an active fluid confined between two walls, showing that the vortex size increases with the separation between the walls, H. (c) The average velocity correlations as a function of distance in the horizontal plane, showing that the minimum of the correlation function shifts to the right (i.e., vortex size increases), as the distance between the walls is increased. At large values of H (e.g., $H = 50$), there is no well defined vortex size. (d) Vortex size as a function of channel height. At small channel heights, the vortex size is larger than the channel height, but as the height increases, the vortex size falls below the height.

[Fig. 2(a)]. The nematic order is high near the walls and low in the middle of the channel, while the nematic director forms an oblique angle with the walls (Supplemental Material [47]), in agreement with experiments [29]. An alternate pathway to this uniform self-pumping state is through the destabilization of a weakly ordered nematic state by a combination of fluctuations in the degree of nematic order and splay deformations, as shown by the stability analysis in [58]. The phenomenology observed on increasing both the channel dimensions commensurately is analogous to the behavior of a 2D confined system—the flows develop components perpendicular to the channel axis at weaker confinements [Fig. 2(c)], and gradually lose their self-pumping nature [diagonals of Figs. 2(d) and 2(e)].

Increasing the channel dimensions *incommensurately* reveals an intriguing behavior that is unique to 3D. Starting from a strongly confined system with a symmetric cross section and uniform coherent flow [Fig. 2(a)], increasing either channel dimension destroys the self-pumping nature of the flow [Fig. 2(b)]. An analogy to 2D systems would suggest that the emergent flows continue to lose coherence as the channel dimensions are increased [53]. However, starting from a channel with a high aspect ratio cross section [e.g., Fig. 2(b)], increasing the size of one dimension to lower the aspect ratio *restores* self-pumping [Fig. 2(c)]. This is because weakening the confinement allows the flows to satisfy incompressibility by spilling into the third (z) dimension rather than by forming closed loops in the (xy) plane (Supplemental Material [47]). Note that the flows in this case are not uniform along the channel axis, and resemble the flows observed in experiments [29].

To understand this novel effect of confinement in a 3D system, we consider a simpler confinement geometry: a pair of walls separated by a distance H [Fig. 1(d)]. The emergent flows in this case are composed of swirling vortices, with a vortex size that increases with confinement size H [Figs. 3(a) and 3(b)]. A similar increase of vortex size with the confinement length scale has been reported in suspensions of microscopic swimmers [59], and in instabilities of nematically ordered systems [58].

Our results show that coherent flows in channels emerge when the vortices generated by one pair of opposing walls are curtailed by the other pair of walls. Comparing the vortex sizes in Fig. 3(d) with the boundaries of the phase diagram for coherent flow in Figs. 2(d) and 2(e) supports this argument: for all confinement geometries with coherent flows, the confinement length in each dimension is smaller than the size of the vortex induced by confinement in the other dimension. Since the vortex size increases with confinement length, this condition simplifies to the following condition for

coherent flow: the larger confinement dimension has to be smaller than the size of the vortex induced by the smaller confinement dimension. For example, consider a channel with width W and height H, such that $W \geq H$. For one pair of channel walls separated by H in the z direction, the vortex size in the xy plane is $\ell(H)$. We now introduce a new set of walls separated by W in the y direction. If $W > \ell(H)$, at least one vortex can form in the xy plane, so the emergent flows will not be net pumping. On the other hand, if $W < \ell(H)$, there is not enough space to form a full vortex, so the flows are net pumping. Since $W \geq H$, coherent flow requires $\ell(H) > H$. Note that it is possible to have $\ell(H) < H$ [Fig. 3(d)] at large H. Therefore, there exists a maximum confinement length scale beyond which coherent flows cannot be obtained. For small activities (e.g., $\alpha = 5$), the confinement height at which $\ell(H) = H$ is nearly equal to the height at which there ceases to be a well-defined vortex size [Figs. 3(c) and 3(d)]. For larger activities (e.g., $\alpha = 7$), $\ell(H) = H$ at a confinement height smaller than the height at which the minimum of the velocity correlation function disappears [Fig. 3(d)].

Experiments on bacterial suspensions confined in 2D channels have reported a similar requirement for existence of spontaneous flows; coherent flows were obtained when the width of the channel was smaller than the intrinsic bulk vortex size, while full vortices and no coherent flows resulted when the width of the channel was larger than this emergent length scale [18]. Note, however, that even 3D channels with square cross sections fundamentally differ from 2D channels: to obtain coherent flows, it is not sufficient that each confinement dimension is smaller than a bulk length scale. Rather, each confinement dimension has to be smaller than the corresponding confinement-induced length scale.

The negative velocity correlations and well-defined vortex sizes in our numerical results [Fig. 3(c)] arise from a complex nonlinear coupling between active flows and hydrodynamic screening. However, we can understand their system-size dependence by considering the following simple model. We approximate the nonlinear effects of flow on the dynamics of the nematic order as a stochastic Gaussian white noise $\Gamma_{\alpha\beta}$, so that $\partial_t Q_{\alpha\beta} = -\gamma Q_{\alpha\beta} + \kappa\nabla^2 Q_{\alpha\beta} + \sqrt{\Delta_\Gamma}\Gamma_{\alpha\beta}$. Let us compute the velocity correlations in the isotropic system confined within walls separated by H. Let $\vec{r}_{||}$ denote position in the xy plane, and z denote position along the confinement dimension. Then, the velocity correlations in the unconfined directions are of the form (Supplemental Material [47])

$$\lim_{|\vec{r}_{||}-\vec{r}'_{||}|\to\infty} \langle u_\alpha(\vec{r}_{||},z,t)u_\alpha(\vec{r}'_{||},z,t)\rangle_0 = \frac{\sqrt{2}\pi^2\alpha^2\Delta_\Gamma}{\gamma\eta^2}\sqrt{\frac{H}{|\vec{r}_{||}-\vec{r}'_{||}|}}\exp\left(-\frac{\pi|\vec{r}_{||}-\vec{r}'_{||}|}{H}\right). \quad (3)$$

Thus, the velocity correlation length in the isotropic state is H/π. Above the flow alignment instability, the nonlinear dynamics give rise to a nontrivial dependence on confinement not captured by this simple analysis.

Conclusions.—In summary, we have shown that an isotropic suspension of extensile rodlike units develops spontaneous flows due to a hydrodynamic instability that couples extensile activity and shear alignment. The size of the vortices generated by this instability depends on the strength of confinement, and coherent flows arise when each confinement dimension is smaller than the size of vortices induced by confinement in the other dimension. This requirement results in aspect-ratio-dependent self-pumping, as observed in recent experiments [29]. Crucially, the minimal nature of our model establishes that this phenomenon is generic to all shear-aligning extensile 3D active systems.

The range of channel sizes that allow net pumping flows can be tuned by controlling material parameters such as activity and diffusion rates, to regulate the velocity correlations. However, the nature of the flow depends on a competition between spontaneous flows generated by the flow alignment instability and destabilization of these flows due to the generic hydrodynamic instability [46,58], and thus arise only in a "sweet spot" of material parameters. If activity or system size is too small, the system is below the flow alignment instability and there are no flows; if the activity or system size is too large, the flows are turbulent. If the material parameters are such that the correlation length $\ell(H)$ is smaller than the confinement size H for all activities high enough to generate spontaneous flows, emergent flows can never be coherent.

Our numerical solutions suggest that the aspect-ratio dependence of coherent flows can be roughly predicted by examining the effect of confinement in each dimension independently. This simple deconstruction is surprising, since active systems are typically highly sensitive to boundaries. Moreover, while the predicted aspect-ratio-dependence of coherent flow is consistent with existing experiments [29], experiments have not yet observed an upper limit to the overall size of the channel cross section that allows coherent flow. Since this maximum size arises due to the predicted sublinear dependence of vortex size on the confinement length scale $\ell(H)$ [Fig. 3(d)], experimentally measuring the size of the largest vortices as a function of confinement dimensions would be the next step toward testing the hydrodynamic theory. To maximize the generality of our conclusions, the hydrodynamic theory we presented here contains only the minimal ingredients for generating the behavior observed in experiments. The theory that most accurately models the experimental system may have additional features. For example, active forces resulting from higher-order gradients of the nematic order could lead to additional instabilities in highly confined geometries [60], and contribute to the loss of coherence observed in high-aspect-ratio channels.

We acknowledge support from the Brandeis Center for Bioinspired Soft Materials, an NSF MRSEC, DMR-1420382 and DMR-2011846 (MV, AB, MFH), DMR-1855914 (M. F. H.), and BSF-2014279 (M. V. and A. B.). Computational resources were provided by NSF XSEDE allocation TG-MCB090163 (Stampede) and the Brandeis HPCC which is partially supported by DMR-MRSEC 2011486.

Note added.—We note that recently, a related insightful but complementary paper appeared that also describes numerical computation of flow states in 3D channels [53]. There, the authors report a loss of coherence of flows when the width of the channel is increased at fixed height, yielding a phenomenology analogous to that of confined 2D active fluids. Our work provides a more comprehensive understanding of the dependence of coherent flow on channel aspect ratio, and thus shows that confined 3D active fluids are fundamentally different from confined 2D active fluids. Further, the analytical investigations described here elucidate the interplay between the system-size dependence of the correlation length and coherent flow. Finally, our work shows that the aspect ratio dependence of coherent flows depends on material parameters, and thus is not an immutable constraint.

[1] S. Ramaswamy, Annu. Rev. Condens. Matter Phys. **1**, 323 (2010).
[2] M. C. Marchetti, J. F. Joanny, S. Ramaswamy, T. B. Liverpool, J. Prost, M. Rao, and R. A. Simha, Rev. Mod. Phys. **85**, 1143 (2013).
[3] J. Elgeti, R. Winkler, and G. Gompper, Rep. Prog. Phys. **78**, 056601 (2015).
[4] C. Bechinger, R. Di Leonardo, H. Löwen, C. Reichhardt, G. Volpe, and G. Volpe, Rev. Mod. Phys. **88**, 045006 (2016).
[5] A. Zottl and H. Stark, J. Phys. Condens. Matter **28**, 253001 (2016).
[6] J. Elgeti and G. Gompper, Eur. Phys. J. Special Topics **225**, 2333 (2016).
[7] N. Yoshinaga, J. Phys. Soc. Jpn. **86**, 101009 (2017).
[8] D. Saintillan, Annu. Rev. Fluid Mech. **50**, 563 (2018).
[9] U. Seifert, Annu. Rev. Condens. Matter Phys. **10**, 171 (2019).
[10] G. D. Magistris and D. Marenduzzo, Physica (Amsterdam) **418A**, 65 (2015).
[11] A. Doostmohammadi, J. Ignés-Mullol, J. M. Yeomans, and F. Sagués, Nat. Commun. **9**, 3246 (2018).
[12] É. Fodor and M. C. Marchetti, Physica (Amsterdam) **504A**, 106 (2018).
[13] M. Bär, R. Großmann, S. Heidenreich, and F. Peruani, Annu. Rev. Condens. Matter Phys. **11**, 441 (2020).
[14] M. R. Shaebani, A. Wysocki, R. G. Winkler, G. Gompper, and H. Rieger, Nat. Rev. Phys. **2**, 181 (2020).
[15] R. Voituriez, J. F. Joanny, and J. Prost, Europhys. Lett. **70**, 404 (2005).
[16] F. G. Woodhouse and R. E. Goldstein, Phys. Rev. Lett. **109**, 168105 (2012).
[17] H. Wioland, F. G. Woodhouse, J. Dunkel, J. O. Kessler, and R. E. Goldstein, Phys. Rev. Lett. **110**, 268102 (2013).
[18] H. Wioland, E. Lushi, and R. E. Goldstein, New J. Phys. **18**, 075002 (2016).
[19] A. Baskaran and M. C. Marchetti, Proc. Natl. Acad. Sci. U.S.A. **106**, 15567 (2009).
[20] E. Lushi, H. Wioland, and R. E. Goldstein, Proc. Natl. Acad. Sci. U.S.A. **111**, 9733 (2014).
[21] D. L. Koch and G. Subramanian, Annu. Rev. Fluid Mech. **43**, 637 (2011).
[22] H. M. López, J. Gachelin, C. Douarche, H. Auradou, and E. Clément, Phys. Rev. Lett. **115**, 028301 (2015).
[23] A. Sokolov and I. S. Aranson, Phys. Rev. Lett. **109**, 248109 (2012).
[24] G. Duclos, C. Blanch-Mercader, V. Yashunsky, G. Salbreux, J.-F. Joanny, J. Prost, and P. Silberzan, Nat. Phys. **14**, 728 (2018).
[25] W. Xi, T. B. Saw, D. Delacour, C. T. Lim, and B. Ladoux, Nat. Rev. Mater. **4**, 23 (2019).
[26] D. Needleman and Z. Dogic, Nat. Rev. Mater. **2**, 17048 (2017).
[27] F. Jülicher, K. Kruse, J. Prost, and J.-F. Joanny, Phys. Rep. **449**, 3 (2007).
[28] T. Sanchez, D. T. N. Chen, S. J. DeCamp, M. Heymann, and Z. Dogic, Nature (London) **491**, 431 (2012).
[29] K.-T. Wu, J. B. Hishamunda, D. T. N. Chen, S. J. DeCamp, Y.-W. Chang, A. Fernández-Nieves, S. Fraden, and Z. Dogic, Science **355**, 1262 (2017).
[30] S. P. Thampi, A. Doostmohammadi, R. Golestanian, and J. M. Yeomans, Europhys. Lett. **112**, 28004 (2015).
[31] D. Saintillan and M. J. Shelley, Phys. Rev. Lett. **99**, 058102 (2007).
[32] D. Saintillan and M. J. Shelley, Phys. Fluids **20**, 123304 (2008).
[33] T. Ishikawa, J. R. Soc., Interface **6**, 815 (2009).
[34] G. Subramanian and D. L. Koch, J. Fluid Mech. **632**, 359 (2009).
[35] C. Hohenegger and M. J. Shelley, Phys. Rev. E **81**, 046311 (2010).
[36] D. Saintillan and M. J. Shelley, J. R. Soc., Interface **9**, 571 (2012).
[37] M. Theillard, R. Alonso-Matilla, and D. Saintillan, Soft Matter **13**, 363 (2017).
[38] V. Mehandia and P. R. Nott, J. Fluid Mech. **595**, 239 (2008).
[39] J. P. Hernandez-Ortiz, C. G. Stoltz, and M. D. Graham, Phys. Rev. Lett. **95**, 204501 (2005).
[40] A. Opathalage, M. M. Norton, M. P. N. Juniper, B. Langeslay, S. A. Aghvami, S. Fraden, and Z. Dogic, Proc. Natl. Acad. Sci. U.S.A. **116**, 4788 (2019).
[41] A. Doostmohammadi and J. M. Yeomans, Eur. Phys. J. Special Topics **227**, 2401 (2019).
[42] T. N. Shendruk, A. Doostmohammadi, K. Thijssen, and J. M. Yeomans, Soft Matter **13**, 3853 (2017).
[43] J. Hardoüin, R. Hughes, A. Doostmohammadi, J. Laurent, T. Lopez-Leon, J. M. Yeomans, J. Ignés-Mullol, and F. Sagués, Commun. Phys. **2**, 121 (2019).
[44] G. I. Taylor, Proc. R. Soc. A **103**, 58 (1923).
[45] F. P. Bretherton, J. Fluid Mech. **14**, 284 (1962).
[46] R. A. Simha and S. Ramaswamy, Phys. Rev. Lett. **89**, 058101 (2002).

[47] See Supplemental Material at http://link.aps.org/supplemental/10.1103/PhysRevLett.125.268003 for details of theory and supplementary numerical results.
[48] M. Doi, S. Edwards, and S. Edwards, *The Theory of Polymer Dynamics*, Comparative Pathobiology—Studies in the Postmodern Theory of Education (Clarendon Press, Oxford, 1988).
[49] N. Van Kampen, in *Stochastic Processes in Physics and Chemistry*, 3rd ed., North-Holland Personal Library, edited by N. Van Kampen (Elsevier, Amsterdam, 2007), pp. 396–421.
[50] A. Baskaran and M. C. Marchetti, J. Stat. Mech. (2010) P04019.
[51] Y. Hatwalne, S. Ramaswamy, M. Rao, and R. A. Simha, Phys. Rev. Lett. **92**, 118101 (2004).
[52] S. Chandragiri, A. Doostmohammadi, J. M. Yeomans, and S. P. Thampi, Soft Matter **15**, 1597 (2019).
[53] S. Chandragiri, A. Doostmohammadi, J. M. Yeomans, and S. P. Thampi, Phys. Rev. Lett. **125**, 148002 (2020).
[54] M. Varghese and A. Baskaran (to be published).
[55] J. Zhao and Q. Wang, J. Sci. Comput. **68**, 1241 (2016).
[56] S. Vanka, J. Comput. Phys. **65**, 138 (1986).
[57] S. A. Edwards and J. M. Yeomans, Europhys. Lett. **85**, 18008 (2009).
[58] P. Chandrakar, M. Varghese, S. A. Aghvami, A. Baskaran, Z. Dogic, and G. Duclos,arXiv:2007.03017 [Phys. Rev. Lett. (to be published)].
[59] J. P. Hernandez-Ortiz, P. T. Underhill, and M. D. Graham, J. Phys. Condens. Matter **21**, 204107 (2009).
[60] A. Maitra, P. Srivastava, M. C. Marchetti, J. S. Lintuvuori, S. Ramaswamy, and M. Lenz, Proc. Natl. Acad. Sci. U.S.A. **115**, 6934 (2018).